Los Alamos NATIONAL LABORATORY EST.1943

LA-UR-15-25174 (Accepted Manuscript)

Reactive transport of uranium in fractured crystalline rock: Upscaling in time and distance

Dittrich, Timothy M.

Provided by the author(s) and the Los Alamos National Laboratory (2016-04-06).

To be published in: Journal of Environmental Management

DOI to publisher's version: 10.1016/j.jenvman.2015.09.014

Permalink to record: http://permalink.lanl.gov/object/view?what=info:lanl-repo/lareport/LA-UR-15-25174

Disclaimer:
Approved for public release. Los Alamos National Laboratory, an affirmative action/equal opportunity employer, is operated by the Los Alamos National Security, LLC for the National Nuclear Security Administration of the U.S. Department of Energy under contract DE-AC52-06NA25396. Los Alamos National Laboratory strongly supports academic freedom and a researcher's right to publish; as an institution, however, the Laboratory does not endorse the viewpoint of a publication or guarantee its technical correctness.

RESEARCH LIBRARY

Reactive Transport of Uranium in Fractured Crystalline Rock: Upscaling in Time and Distance

Timothy M. Dittrich[a,*] and Paul W. Reimus[a]

[a] *Earth and Environmental Sciences Division, Los Alamos National Laboratory, Los Alamos, NM 87545, USA*

** Corresponding author: Los Alamos National Laboratory, P.O. Box 1663, Mail Stop J966, Los Alamos, NM 87545*

Tel: 575-234-5538, Fax: 505-606-2258. E-mail address: timdittrich@lanl.gov

Abstract

Batch adsorption and breakthrough column experiments were conducted to evaluate uranium transport through altered material that fills fractures in a granite rock system at the Grimsel Test Site in Switzerland at pH 6.9 and 7.9. The role of adsorption and desorption kinetics was evaluated with reactive transport modeling by comparing one-, two-, and three-site models. Emphasis was placed on describing long desorption tails that are important for upscaling in time and distance. The effect of increasing pH in injection solutions was also evaluated. For pH 6.9, a three-site model with forward rate constants between 0.07 and 0.8 mL g^{-1} h^{-1}, reverse rate constants between 0.001 and 0.06 h^{-1}, and site densities of 1.3, 0.104, and 0.026 µmole g^{-1} for 'weak/fast', 'strong/slow', and 'very strong/very slow' sites provided the best fits. For pH 7.9, a three-site model with forward rate constants between 0.05 and 0.8 mL g^{-1} h^{-1}, reverse rate constants between 0.001 and 0.6 h^{-1}, and site densities of 1.3, 0.039, and 0.013 µmole g^{-1} for a 'weak/fast', 'strong/slow', and 'very strong/very slow' sites provided the best fits. Column retardation coefficients (R_d) were 80 for pH 6.9 and 10.3 for pH 7.9. Model parameters determined from the batch and column experiments were used in 50 year large-scale simulations for continuous and pulse injections and indicated that a three-site model is necessary at pH 6.9, although a K_d-type equilibrium partition model with one-site was adequate for large scale predictions at pH 7.9. Batch experiments were useful for predicting early breakthrough times in the columns while column experiments helped differentiate the relative importance of sorption sites and desorption rate constants on transport.

Keywords: uranium, Grimsel granodiorite, reactive transport modeling, sorption kinetics, rate coefficients, column experiments

1. Introduction

Providing reliable predictions for risk assessments of nuclear waste repository designs is a challenge due to difficulties in upscaling in time and distance. Our work focuses on refining an experimental and reactive transport modeling approach for describing and parameterizing upscaled radionuclide transport in a more robust and less conservative manner than a simple K_d-type equilibrium partitioning model without resorting to a full geochemical description of the rock-water-radionuclide system. K_d-type models are often overly conservative and do not take full credit for all the retardation processes that may be occurring in a given system (Davis et al., 2005; Morel and Hering, 1993; Payne et al., 2013) – this can lead to overly conservative repository system designs that are prohibitively expensive. Detailed geochemical models typically account for a large number of reactions but still often miss key site-specific reactions slow reaction rates leading to marginal predictive improvements. The motivation for this work is that each unique system must be investigated for site-specific behaviors, including processes such as slow desorption kinetics and bond-aging phenomena often not accounted for in geochemical models (Boukhalfa et al., 2013; Davis et al., 2004; Dong and Wan, 2014; Mohanty et al., 2014; Nebelung and Brendler, 2010; Waite et al., 2000). While detailed geochemical descriptions remain useful (e.g., Liu et al, 2008), we suggest using a focused set of initial experiments to identify key processes that may require more detailed investigation and also to provide reasonable semi-empirical descriptions of radionuclide transport processes that can be used in performance assessment calculations. These calculations, in turn, can be used to evaluate the need for more detailed process descriptions on a risk-informed basis.

We demonstrate a cost-effective approach of accounting for radionuclide retardation processes in performance assessments, particularly for moderately-adsorbing radionuclides for

which risk estimates can be sensitive to assumptions and uncertainties associated with adsorption and desorption processes. The approach involves conducting breakthrough experiments in small columns that require minimal amounts of geologic materials, with emphasis on interrogating and parameterizing long-term desorption behavior that can strongly influence large-scale transport behavior. Preliminary experiments (Dittrich and Reimus, 2015; Wang et al., 2013b) were expanded upon to incorporate longer desorption periods and tighter control of pH conditions to improve efforts in upscaling to the longer time scales needed for repository design and reliable risk assessments.

Uranium is likely to be an important radionuclide in risk or dose calculations for most geologic repository systems for unreprocessed spent nuclear fuel due to its large inventory and relatively weak adsorption in many geochemical environments. Uranium adsorption partition coefficients (K_d values) for many different minerals have been reported to vary over several orders of magnitude between pH 7 and 9 (Davis and Curtis, 2003; Echevarria et al, 2001; Joseph et al., 2013; Waite et al., 1994), with essentially zero K_d at pH of 9 or higher. For a given pCO_2, U exhibits much stronger adsorption at the low end of this pH range because of the greater abundance of positively-charged uranyl species (UO_2^{2+} and $UO_2(OH)^+$) and the lesser abundance of nonsorbing neutral and negatively-charged uranyl carbonate or uranyl-Ca/Mg-carbonate complexes at neutral pH (Dittrich and Reimus, 2015).

Our current effort has focused on U transport in a saturated, fractured crystalline rock system, using the Grimsel Test Site (GTS) in Switzerland as a source of geologic materials due to extensive field and laboratory experimentation and characterization (Geckeis et al., 2004; Möri et al., 2003). We have lowered the pH of the site-specific groundwater to be more consistent with other crystalline rock systems and to provide greater amounts of U adsorption (U sorption is

negligible at ambient GTS pH of ~9). We also conducted our experiments under oxidizing conditions to avoid redox processes that would further complicate U transport behavior, although we recognize that many deep crystalline rock environments are inherently reducing and such redox processes may ultimately need to be considered for a redox-sensitive element like U (Huber et al., 2011). The Grimsel granodiorite system was chosen for this study for several reasons: (1) it is representative of a generic crystalline rock repository, (2) field transport experiments with U and other radionuclides are being conducted at the site, and (3) the Los Alamos National Laboratory is involved in a formal collaboration with the Colloid Formation and Migration project at the GTS.

2. Materials and Methods

2.1. Groundwater and Uranium

The groundwater used in all experiments was a synthetic Grimsel ground water (SGGW) made by adding $NaSO_4$, KCl, $MgCO_3$, $NaHCO_3$, $CaCl_2$, and H_4SiO_4 to high purity water with the exact recipe provided in Supplemental Materials (Table A1). The SGGW represents the water chemistry in the shear zone at the GTS (Huber et al., 2011; Missana et al., 2004) with additional Mg and carbonate that would be contributed from an engineered barrier consisting of FEBEX bentonite (ENRESA, 1998). The SGGW has a pH range of 8.8-9.1, which was lowered to pH 6.9 and 7.9 with N-morpholino-ethanesulfonic acid (MES) and remained stable for at least 6 months (Wang et al., 2014a; 2013b). These pH values allowed for comparison with similar experiments conducted at the GTS.

A 6.5 µM U solution was made by spiking SGGW with a combination of ^{233}U (Eckert and Ziegler) and natural uranium (SpexCertiPrep, ICP-MS standard). Uranium-bearing species in SGGW were calculated using PHREEQC (Parkhurst and Appelo, 2013) and the llnl.dat database

(Johnson, 2010) with the addition of uranyl-calcium-carbonate and uranyl-magnesium-carbonate complexation constants from Dong and Brooks (2006) and are shown in Table A2. Tritium was co-injected with U in all column experiments as a conservative tracer to provide a means to quantify residence times and dispersivity in the columns. This low concentration of U was selected to model a small concentration of mobile U after attenuation from transport through an engineered barrier and to ensure U chemical stability in the SGGW.

2.2. Fracture Fill Material

Fracture fill material (also known as FFM or fault gouge) from a highly altered fracture in a granite/granodiorite formation was collected during coring operations at the GTS. Samples (< 1 µm to 15 cm pieces) were shipped to Los Alamos National Laboratory and all pieces less than 1 cm in size were combined and crushed, sorted, and rinsed in high-purity water to removal all fines. The 150-355 µm size fraction was used in all experiments. Quantitative x-ray diffraction (QXRD) mineralogy shows that the FFM is 34% albite, 31% biotite, 16% muscovite, 13% quartz, 5% microcline, and 1% or less of smectite and calcite. Previous publications have shown that the material used represents the surfaces of the fractures at the GTS well and these detaisl and SEM images are shown in Dittrich et al. (2015a) and Dittrich et al. (2015b). Bulk chemical analysis by x-ray florescence (XRF) has also been previously reported (Dittrich and Reimus, 2015). Surface area was 0.23 m^2 g^{-1} as measured by krypton-BET (Micromeritics Analytical Services).

2.3. Analytical Measurements

Radionuclide concentrations were measured by liquid scintillation counting, or LSC (Perkin Elmer Tri-Carb 2550) for 30 minutes with Ultima Gold AB (Packard) liquid scintillation cocktail

with energy ranges of 0-20 keV for tritium and 100-260 keV for U. pH measurements were made using a pH meter (Orion Model 290) and a glass pH electrode (Fisher AccupHast).

2.4. Column Transport Experiments

Column transport experiments were conducted by injecting pH-adjusted SGGW spiked with U and tritium with upward flow through 6 cm long Teflon® mini-columns filled with 5.0 g of FFM. All experiments were conducted in duplicate. Tubing, syringes, and fittings were made of Teflon® to reduce sorption artifacts and a 75 µm PEEK screen retained material in the columns. Construction details are provided elsewhere (Dittrich et al., 2015c; Dittrich and Reimus, 2014). Teflon® syringes (Torviq, TS-50, 50 mL) with syringe pumps (KD Scientific, Model 100) set to 0.3 mL h^{-1} were used to eliminate interactions between U and the syringes, which have been observed in column experiments with polypropylene syringes (Kersting et al., 2012). 3-way stopcocks allowed for refilling syringes and switching solutions while minimizing flow and pressure disturbances. Effluent samples were collected in an enclosed fraction collector (Gilson, FC-220) filled with 13 × 100 mm polystyrene test tubes (Figure A1).

Control experiments with empty columns were conducted to identify potential interactions between U and flow system materials. The columns were initially flushed with U-free SGGW for 7 days to ensure the effluent pH stabilized within 0.1 pH unit of U solutions. The influent solution was then switched to SGGW containing U and tritium.

The actual flow rate through the columns (~0.28 mL h^{-1}) was determined by weighing test tubes before and after sample collection. U and tritium activity were measured in every sample. Syringes were refilled several times before changing to U-free solution. pH was measured for one of the duplicate columns. Great care was taken to ensure that pH remained as steady as possible since subtle changes in pH can result in significant and rapid changes in U adsorption

(Dittrich and Reimus, 2013; Wang et al., 2013b). Late in each column experiment, however, the pH was purposely changed to induce U desorption and provide additional insights into the desorption process. pH 6.9 experiments were subjected to U-free SGGW of pH 6.9, 9.0, and 1.2; whereas, pH 7.9 experiments were only subjected to 7.9 pH U-free SGGW and then 1.2 pH HCl to release U and allow for a mass balance calculation. The experimental conditions and injection times/volumes are summarized in Table 1.

2.5. Batch Adsorption/Desorption Experiments

Batch experiments were conducted at pH 6.9 and 7.9 in fluorinated ethylene propylene (FEP) centrifuge tubes with 10 ml of U-spiked SGGW placed in contact with 0, 0.2, 0.5, or 1.0 g of FFM oscillated on an orbital shaker (VWR Scientific, DS-500) at 180 RPM. All experiments were conducted in duplicate. Samples (0.75 mL) were collected after 10, 100, 1000, 5900, 17200, and 18600 minutes. After 18600 minutes, all SGGW except for ~0.5 ml was removed from each centrifuge tube and replaced with 9.5 ml of U-free SGGW. Samples were collected after 10, 100, 1000, 8300, and 17100 minutes to observe the U desorption behavior.

2.6. Modeling Approach

A multisite/multirate reaction model (Dittrich and Reimus, 2015; Wang et al., 2013a) was used to interpret the column and batch data. The batch experiment governing equations are:

$$\frac{\partial s_i}{\partial t} = k_{fi} c \left(1 - \frac{s_i}{s_{mi}}\right) - k_{ri} s_i \quad (1)$$

$$\frac{\partial c}{\partial t} = \frac{M}{V}\left[-\sum_i k_{fi} c \left(1 - \frac{s_i}{s_{mi}}\right) + \sum_i k_{ri} s_i\right] \quad (2)$$

where, c = concentration in aqueous phase, mol mL^{-1}
s_i = concentration on surface sorption site i, mol g^{-1}
t = time, h
k_{fi} = adsorption rate constant for sorption site i, ml g^{-1} h^{-1}
k_{ri} = desorption rate constant for site i, h^{-1}
s_{mi} = surface site density (maximum adsorption capacity) for sorption site i, mol g^{-1}

M = mass of solids, g
V = volume of solution, mL.

The column transport governing equations were equation (1) for surface sorption with the following equation for the mobile aqueous phase:

$$\frac{\partial c}{\partial t} = -v\frac{\partial c}{\partial x} + D\frac{\partial^2 c}{\partial x^2} + \frac{\rho_B}{\emptyset}\left[-\sum_i k_{fi} c\left(1 - \frac{s_i}{s_{mi}}\right) + \sum_i k_{ri} s\right] \quad (3)$$

where, v = flow velocity, cm h^{-1}
D = dispersion coefficient, cm^2 h^{-1}
ρ_B = bulk density of solids, g cm^{-3}
ϕ = porosity

Equations (1) and (2) were solved using a 4th-order Runge-Kutta algorithm and equations (1) and (3) were solved simultaneously using an implicit finite-difference algorithm. After estimating v and D by fitting the tritiated water breakthrough curves with no reactions, the U data were fitted by adjusting adsorption and desorption rate constants, number of adsorption sites, and site surface densities. Reaction parameters (k_{fi}, k_{ri}, and s_{mi}) were allowed to be varied for different pH values.

The approach to interpreting the column experiments was to try to match the U breakthrough curve(s) with as few reaction parameters and adsorption site types as possible. The resulting parameters were then compared to the fitted batch adsorption/desorption parameters to gain additional insights into the adsorption and desorption processes.

3. Results

3.1. Breakthrough Column Results

Duplicate control column breakthrough experiments at pH 6.9 and pH 7.9 indicate a slight retention of U even with Teflon® syringes and tubing (Figure A2 in Supplementary Material); however, this retention was much less than in experiments with polypropylene syringes and Tygon® tubing (Dittrich and Reimus, 2015; Kersting et al., 2012). Retention to flow system components at pH 7.9 appeared to be negligible, although the U concentration reached only 90-

95% of its injection concentration in the effluent of both control columns. Importantly, the desorption tails at both pH 6.9 and pH 7.9 matched the tritium curves quite well. Breakthrough data are shown in Figures A3 and A4.

3.1.1. pH 6.9 Model Fits

Model fits of tritium breakthrough data (not shown) indicated a mean column pore volume of 1.4 mL and a Peclet number of 100. A three-site model matched the U breakthrough results well. The U data and model fits are shown in Figure 1, and the reaction parameters corresponding to these fits are listed in Table 2. In order to fit the sudden drop in U concentrations that occurs after the switch to U-free water (believed to be due to a subtle drop in alkalinity), a minor decrease in the U desorption rate constant for the first sorption site was necessary.

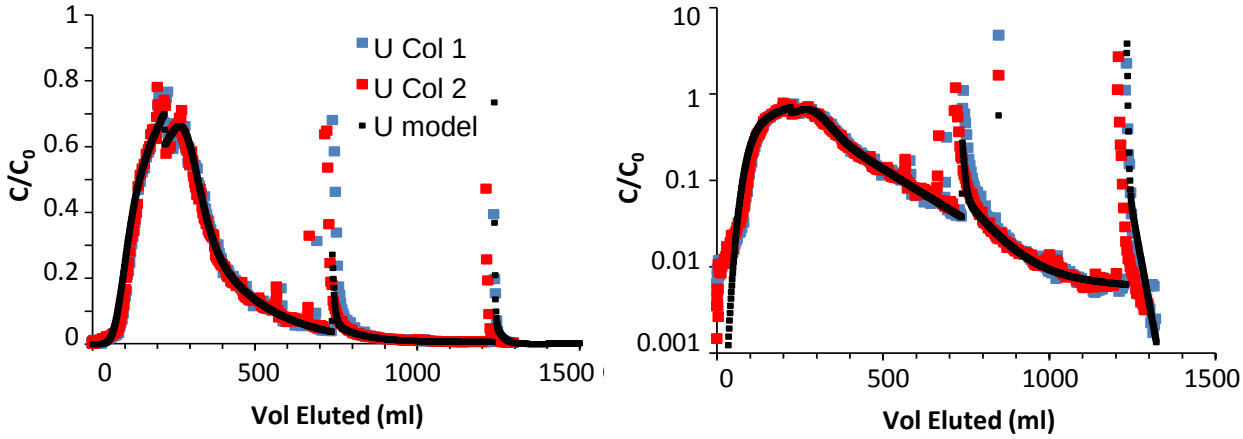

Figure 1. Best fit of three-site model to the duplicate U breakthrough curves in FFM column experiments at pH 6.9, plotted on a linear concentration scale (left) and logarithmic scale (right). Best-fitting reactive transport parameter estimates are listed in Table 2.

3.1.2. pH 7.9 Model Fits

The U breakthrough curves and best model fits in the pH 7.9 column experiments are shown in Figure 2 with reaction parameters listed in Table 3.

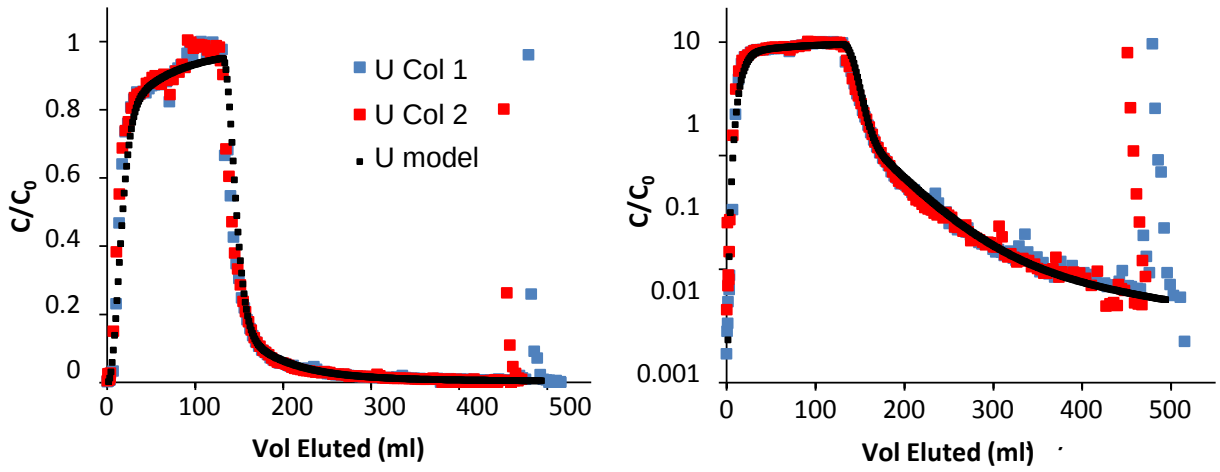

Figure 2. Best fit of three-site model to the duplicate U breakthrough curves in FFM column experiments at pH 7.9, plotted on a linear concentration scale (left) and logarithmic scale (right). Best-fitting reactive transport parameter estimates are listed in Table 3. Note that the change to pH 1 at around 490 ml was not modeled.

As with the pH 6.9 column experiments, three adsorption sites were found to be necessary to obtain a good match to the U breakthrough curves at pH 7.9. Comparison of the desorption tails indicate more rapid U desorption occurred at pH 7.9 than at pH 6.9. Over 97% of the U was calculated to be recovered before the pH 1 flush was started, and a log-log extrapolation of the tail of the pH 7.9 breakthrough curve predicts that about 99% would have been recovered had the log-log trend continued to infinite time. The mass balance after the pH 1 flush was slightly greater than 100% (101% and 100.7% in columns 1 and 2, respectively), which suggests that the U recoveries at the end of the pH 7.9 portion of the experiment may have been as much as 1% lower than calculated (i.e., there was slightly greater U retention than calculated). This excellent

mass balance closure is well within the precision of our measurements and suggests that systematic errors were less than the 3-5% mass shortfall for pH 6.9 experiments.

3.2. Batch Results and Model Fits

Data from the batch experiments (Figure 3) were fitted with a one-site adsorption model (pH 6.9 only) and a three-site adsorption model (both pHs) and Table A3 lists the best-fitting parameters.

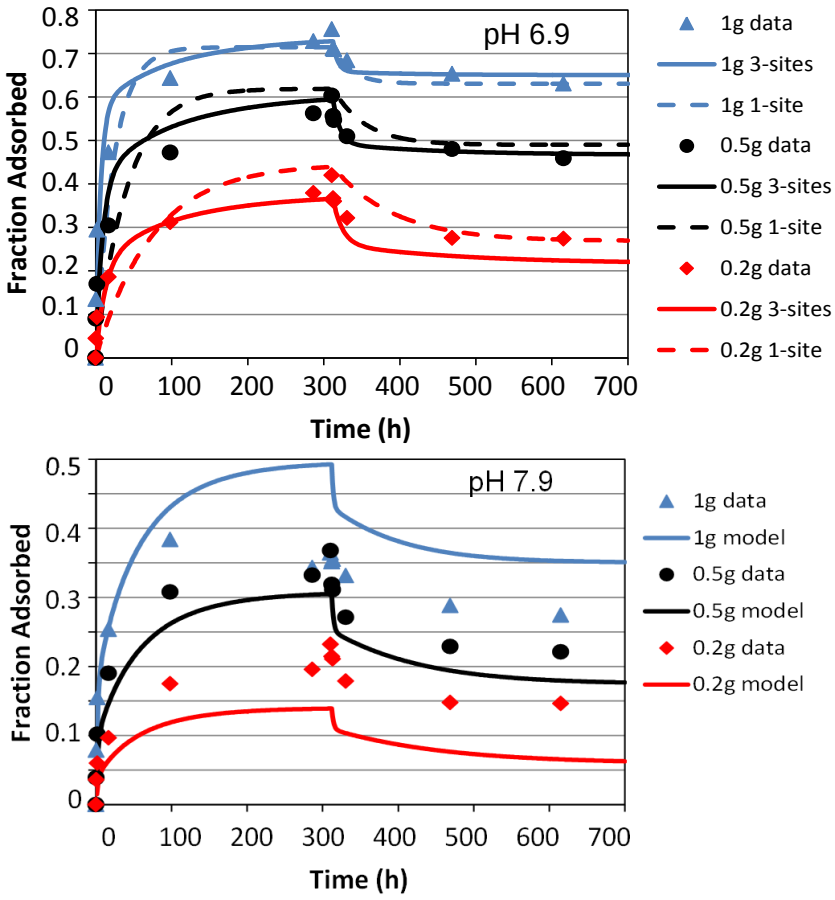

Figure 3. FFM batch adsorption and desorption data at pH 6.9 (top) and pH 7.9 (bottom), with 3-site and 1-site model fits to the pH 6.9 data and a 3-site model fit to the pH 7.9 data. Legend indicates grams of FFM material per 10 ml of initial solution. Data points are averages of duplicate experiments.

These fits were constrained by assuming that the same reaction parameters must apply to all the solid-to-solution ratios, which is why the model over-predicts the observed sorption at the

highest ratio for pH 7.9 and under-predicts the observed sorption at the lowest ratio for this pH. The three-site model is superior to a one-site model, which is consistent with the column experiments; however, the batch adsorption reaction rate constants are somewhat slower than the column rate constants and the batch desorption rate constants are somewhat faster.

Model predictions for the batch experiments using the best-fit column experiment parameters are shown in Figure A5. The column parameters at pH 6.9 provide reasonably good matches to the batch results (although the adsorption rates are over-predicted), but the column parameters at pH 7.9 significantly underpredict the batch results at the two smaller batch solid-to-solution ratios. The highest batch solid-to-solution ratio resulted in the best match, presumably because the solid-to-solution ratio in the columns was much larger than in any of the batch experiments (approximately 5 g to 2.5 mL).

4. Discussion

4.1. Number of binding sites (Comparison of one-, two- and three-site models)

Early breakthrough of U is dictated primarily by the adsorption and desorption rate constants of the first adsorption site, which is the site with the highest surface density and the fastest rate constants. The ratio of the adsorption to desorption rate constant of this site dictates the timing of the U arrival, and the value of the adsorption rate constant dictates the slope of the arrival, with a faster rate constant resulting in a steeper slope. The second and third sites have slower rate constants than the first site. Without a second site, the modeled U concentration would rapidly rise to $C/C_0 = 1$ and it would also rapidly decrease from $C/C_0 = 1$ after U-free water is introduced to the column. This result is illustrated in Figure 4 for the pH 6.9 column experiment. A second, slower site helps keep the U concentration from reaching $C/C_0 = 1$ while still allowing a relatively rapid rise in concentration, and it also helps fit the tail of the U breakthrough curve.

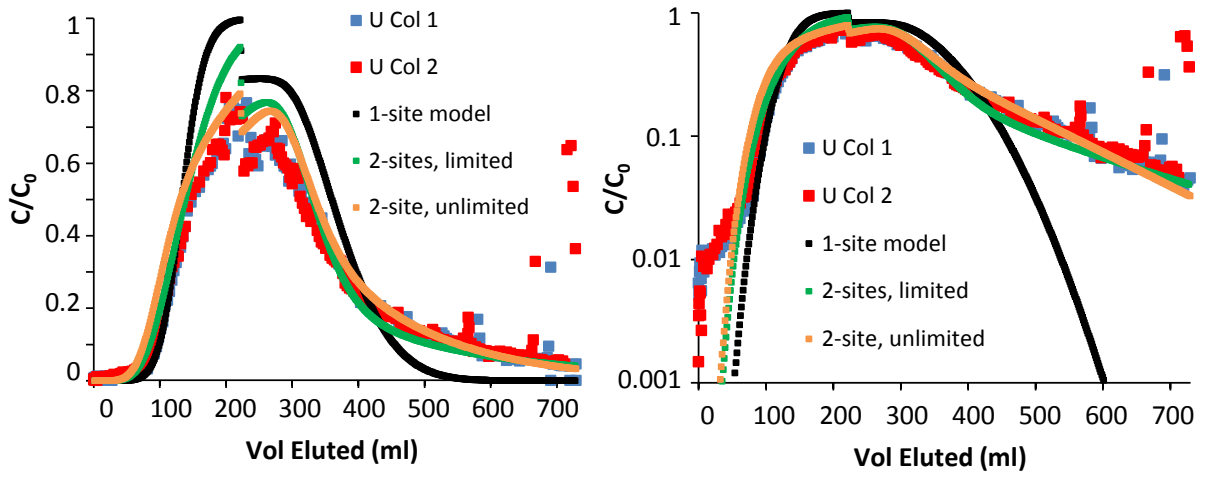

Figure 4. One-site and two-site model fits for duplicate U breakthrough curves in FFM column experiments at pH 6.9. The one-site model has an adsorption rate constant of 3.0 ml/g-h and a desorption rate constant of 0.066 h^{-1}. The two-site limited model has adsorption rate constants of 2.1 and 0.12 ml/g-h for the first and second sites, respectively, and desorption rate constants of 0.07 and 0.0016 h^{-1} for the two sites, with a second site density of 0.11 μmol/g. The two-site unlimited model has adsorption rate constants of 2.1 and 0.07 ml/g-h and desorption rate constants of 0.07 and 0.0025 h^{-1}, respectively (with a second site density of 0.39 μmol/g).

Two separate curves are shown for the two-site model in Figure 4; comparing a large and limited second site surface density. The rate constants and surface site density of the second site can be varied systematically to achieve similar fits because these parameters are correlated, resulting in nonuniqueness of the best-fitting parameter estimates. When the density of the second site is decreased, the adsorption rate constant can be increased to achieve similar amounts of adsorption to the second site. A limit is reached where the fit degrades significantly after the site density drops below a critical value (or the adsorption rate constant rises above a certain value). The two-site model curve with a more limited number of second sites is a poorer fit to the U breakthrough curve because the second site density is lower than the critical value yielding reasonably good fits. The best fits can always be obtained with a very large number of sites

because the adsorption rate constants can always be adjusted to provide good matches to the data.

While the two-site model curves of Figure 4 are clearly an improvement over the single-site curve, they still fail to fully explain the observed data. As Figure 1 shows, the addition of a third site helps achieve an excellent match to the data. In effect, the third site serves as an irreversible sink for the U over the time scale of pH 6.9 portion of the experiment. This adjusts the model curve downward to correct for the over-prediction of concentrations near the peak of the breakthrough curve. The third site did not have to be specified as irreversible – it merely must have a small enough desorption rate constant to effectively retain most of the adsorbed U for the remainder of the pH 6.9 portion of the experiment after the U-free water was introduced. Note that although Table 2 lists two subsets of the third site (3a and 3b), these are effectively the same site during the pH 6.9 and 9.0 portion of the experiment because they have the same desorption rate constant - their adsorption rate constants can be added to obtain an overall adsorption rate constant for a combined site. Site 3b is specified only to achieve a match to the pH ~1 portion of the experiment. It should also be noted that the same negative correlation between the adsorption rate constant and surface site density mentioned above for the second site also applies to the third site – the third site density can be decreased with a corresponding increase in adsorption rate constant to achieve a similar fit. This results in a degree of nonuniqueness in the model fits. There is, however, a lower surface site density limit below which the fits degrade significantly. The model curve of Figure 1 during the pH 6.9 portion of the column experiments is quite insensitive to the desorption rate constant of the third site, provided the rate constant is less than a critical upper limit above which a significant amount of the U adsorbed to the third site begins to desorb over the time scale of the experiment.

4.2. Column and batch result comparison

The adsorbed U fractions in the batch experiments at pH 7.9 were expected to decrease significantly as the solid-to-solution ratios were decreased because of the relatively weak adsorption at this pH, but the decrease is not nearly as great as the model can fit or predict. We suspect that there may have been some experimental artifacts that either suppressed U adsorption at the highest solid-to-solution ratio at pH 7.9 or, more likely, increased it at the lower solid-to-solution ratios. The most likely such artifact would be a lower alkalinity in the reactors with lower solid-to-solution ratios, which would increase the adsorption in these reactors. We did not measure the alkalinity due to limited sample volumes. Although the model failed to predict the fractions adsorbed at the two lower solid-to-solution ratios at pH 7.9, the rate and amount *desorbed* in these experiments is actually quite well predicted (much better than at the highest ratio in Figure 3).

The batch experiments were conducted at relatively low solid-to-solution ratios with the hope of interrogating surface site saturations, particularly at the lowest solid-to-solution ratio of 0.2 g to 10 ml. These effects would be manifested by a decrease in the apparent partition coefficient at smaller solid-to-solution ratios, and if observed, they might provide some constraints on the total U adsorption site capacity (i.e., site density) on the FFM surfaces at the experimental pHs, and perhaps some constraints on the site densities of the second and third sites (via model fitting). However, these effects were not observed at either pH. The apparent partition coefficients increased rather than decreased as solid-to-solution ratios decreased at pH 7.9. Table 4 lists the apparent adsorption and desorption partition coefficients in the batch experiments as determined from the final concentrations observed during both the adsorption and desorption phases of the batch experiments. We are left to conclude that the batch experiments did not yield meaningful

constraints on the surface densities of the adsorption sites in the column experiments, and they also seemed to under-predict the adsorption rates observed, especially in the pH 6.9 column experiments. The under-prediction of adsorption rates might be a result of greater mass transfer limitations in the batch experiments due to the grains settling in the reaction vessels despite agitation on the orbital shaker. The estimation process for the rate constants inherently accounts for differences in solid-to-solution ratios in different experiments.

Despite the inability to obtain good constraints on adsorption site densities from the batch experiments and good agreement between the batch and column reaction rate parameters, the batch adsorption partition coefficients predict the arrival times of the U in the column experiments reasonably well at both pHs. Given that the porosity in the columns was about 50%, resulting in a bulk density of about 1.325 g cm^{-3}, the predicted retardation factors in the columns are $1 + 1.325(K_d)/0.5$, or $1 + 2.65(K_d)$. Table A4 lists the column retardation factors, R, calculated using the adsorption partition coefficients of Table 4 (65-71 and 15-31 for pH 6.9 and 7.9, respectively) along with the observed column retardation factors based on when the U concentration reached half its peak concentration (80 and 10, respectively). These results suggest that the batch experiments were useful for predicting when the early arrival of U occurred in the columns. The greater desorption partition coefficients relative to the adsorption coefficients are also consistent with the extended tailing observed in the column experiments, which suggest desorption rates are lower than adsorption rates.

Overall, the batch experiments helped predict the early breakthrough times in the column experiments fairly well but were of limited value in gaining additional insights into the observed U column transport behavior, particularly the slow desorption rates in the columns. Suggested improvements for batch experiments include (1) continually adding more U after some

adsorption has occurred until U adsorption per unit mass of added U clearly decreases, (2) replacing the desorption solution with U-free water multiple times until analytical detection limits are reached to better interrogate slow desorption rate constants, and (3) generally using higher mass to solution ratios to more closely match column or field conditions. The first and second suggestions would help place better constraints on surface site densities of the different sorption sites, which we do not believe were very well constrained by the column experiments. The third suggestion is mainly to avoid artifacts and data scatter that can occur when small sample sizes are used with materials of high mineralogical heterogeneity, which may have been a factor in the batch experiments with the small solid-to-solution ratios.

4.3. Extrapolation of Column Model Results

Figure 5 shows three extrapolations of the pH 6.9 model curve (assuming no increase to pH 9) with three different values of the third site desorption rate constant. The largest value ($0.00013\ h^{-1}$) results in the model curve deviating from the log-linear trend in the tail of the breakthrough curve almost immediately after the end of the pH 6.9 data. The intermediate value ($0.00003\ h^{-1}$) shows a deviation some time after the end of the pH 6.9 data, and the smallest value ($0.000003\ h^{-1}$) shows a deviation occurring at about the U detection limit of our LSC method. While each curve explains the *observed* data equally well, each has significantly different implications for long-term and large-scale transport. As will be shown in Section 4.4, the smaller the desorption rate constant of the third site, the greater will be the predicted retardation of U over large scales.

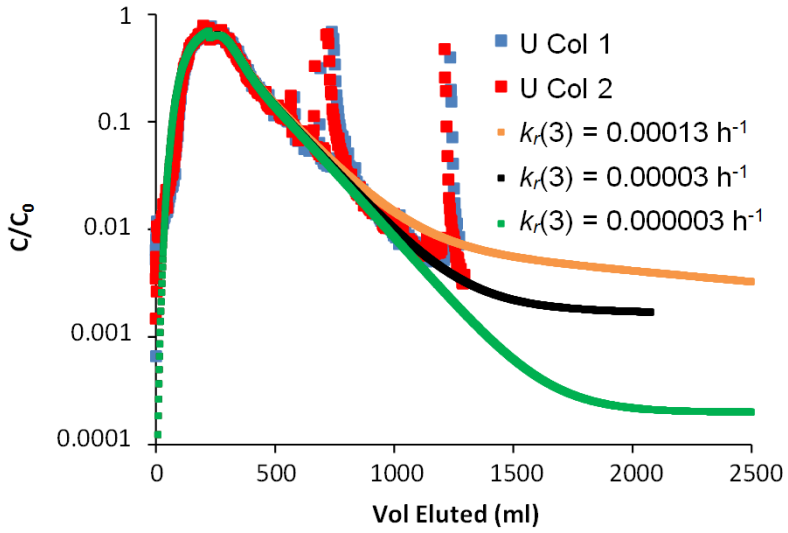

Figure 5. Extrapolations of the model-simulated pH 6.9 U breakthrough curves assuming no pH changes and three different desorption rate constants for the third site, $k_r(3)$. All other parameters are the same as in Table 2. Note that sites 3a and 3b were combined as a single site.

A valid question is: Why was the pH increased to 9 before a deviation was observed in the tail of U breakthrough curve? If one were really trying to interrogate the slowest desorption rates at a pH of 6.9, the logical procedure would be to extend the breakthrough curves until a deviation was observed or until the concentrations drop below detection limits, whichever comes first. If the log-linear tails are simply extrapolated to infinite time, it is predicted that only about 84% of the U would be recovered, with the implication being that over 15% of the U must have a zero desorption rate. Even if a log-log extrapolation is done, which involves some upward curvature of the trend on a log-linear scale, the predicted recovery is only ~91%, and thus 9% of the U is predicted to have a zero desorption rate. In both of these cases, the large-scale retardation of U would be very great because some of the U would be predicted to be irreversibly adsorbed. In reality, it is quite uncertain to make such extrapolations, and it is clearly non-conservative to assume any irreversible adsorption sites without direct evidence – evidence which, almost by

definition, is impossible to obtain without running infinitely long experiments and having extremely low detection limits.

Rather than extend the experiments at pH 6.9, we decided to increase the pH to 9, which is the ambient Grimsel pH, to see how much desorption would be induced by this pH increase. We had previously shown (Kersting et al., 2012) in both batch and column experiments that there was no observable *adsorption* to Grimsel granodiorite at pH 9, so it was expected that raising the pH to 9 would induce considerable desorption. While Figures 1 and 2 show that this clearly occurred, it is interesting that the desorption was not complete (about 8% of the injected U was rapidly desorbed, whereas ~20% of the injected U was retained in the columns when the pH was initially switched to 9). It is even more interesting that the tail occurring after the large spike appears to resume the log-linear trend observed prior to the pH increase. This observation suggests that the trend at pH 6.9 would have likely continued at least until the end of the pH 9 injection, especially when one considers that desorption rates should have been significantly higher at pH 9 than pH 6.9. Thus, we feel confident in using the intermediate value of the third-site desorption rate constant of 0.00003 h^{-1}(Figure 5) as an upper limit for the desorption rate constant of this site *at pH 6.9*.

The fact that there is clearly some slow desorption occurring at pH 9 indicates that while observable adsorption did not occur at this pH in either column or batch experiments (Kersting et al., 2012), U that was adsorbed at lower pHs does not necessarily desorb rapidly when subjected to pH 9 solutions. We considered the possibility that there may be a slow-diffusion component to the release of u from the FFM, but this possibility seems remote given (1) the rapid desorption of a portion of the U mass, which was obviously not diffusion-limited, and (2) the steep slope of the U decrease on a log-log plot after the initial rapid desorption, which was much steeper (slope

of less than -2.5) than would be predicted from a diffusion-dominated process (slope of -1.5, Tsang (1995)).

The pH ~1 flush of the columns resulted in nearly complete recovery of the U from the columns: 95% recovery for Column 1 and 97% for Column 2. This result indicates that systematic errors in the U concentration measurements were relatively small (less than 5%) over the course of the experiments. More importantly, the significant spike in concentrations after introducing the pH 1 solution confirms that there was indeed a significant amount of U remaining on the FFM after the pH 9 solution had been flushing the columns for considerable time. About 6% of the injected U was desorbed during the pH 1 flush in both columns, confirming that the pH 9 flush left behind a significant fraction of the U that was adsorbed to the FFM at the start of the flush (6% of the 20% that was adsorbed at the start of the flush). The lack of complete mass balance closure suggests that it is possible that even the pH 1 flush did not remove all the adsorbed U, although a systematic mass balance error of 3-5% in the experiments was also possible.

4.4. Implications for large-scale transport

To evaluate the implications of the column experiment results over longer time and distance scales, the three-site model was used with the best-fitting reaction parameters of Tables 2 and 3 to simulate large-scale reactive transport for pH 6.9 and 7.9 U contaminated groundwater. Simulations were also conducted using a single fast site with a partition coefficient equal to either the adsorption or desorption K_d value that was experimentally observed at the highest solid-to-solution ratio in the batch experiments (Table 4).

Mean water residence time of 1 year was simulated for a steady input of 6.5 μM U (upper plot) and a 50-year pulse of 6.5 μM U (lower plot). A Peclet number of 120 was used in all

simulations (i.e., minimal dispersion). With a mean residence time of one year and a large Peclet number, the effective U retardation factor is the number of years taken to reach C/C_0 = 0.5 in the continuous-input plots. The three curves of Figure 6 labeled "column *kr*" used identical values of all reaction parameters (i.e., Table 2) except for the desorption rate constant of the third site, for which values of 0.0013, 0.00003, and 0.000003 h^{-1} were used.

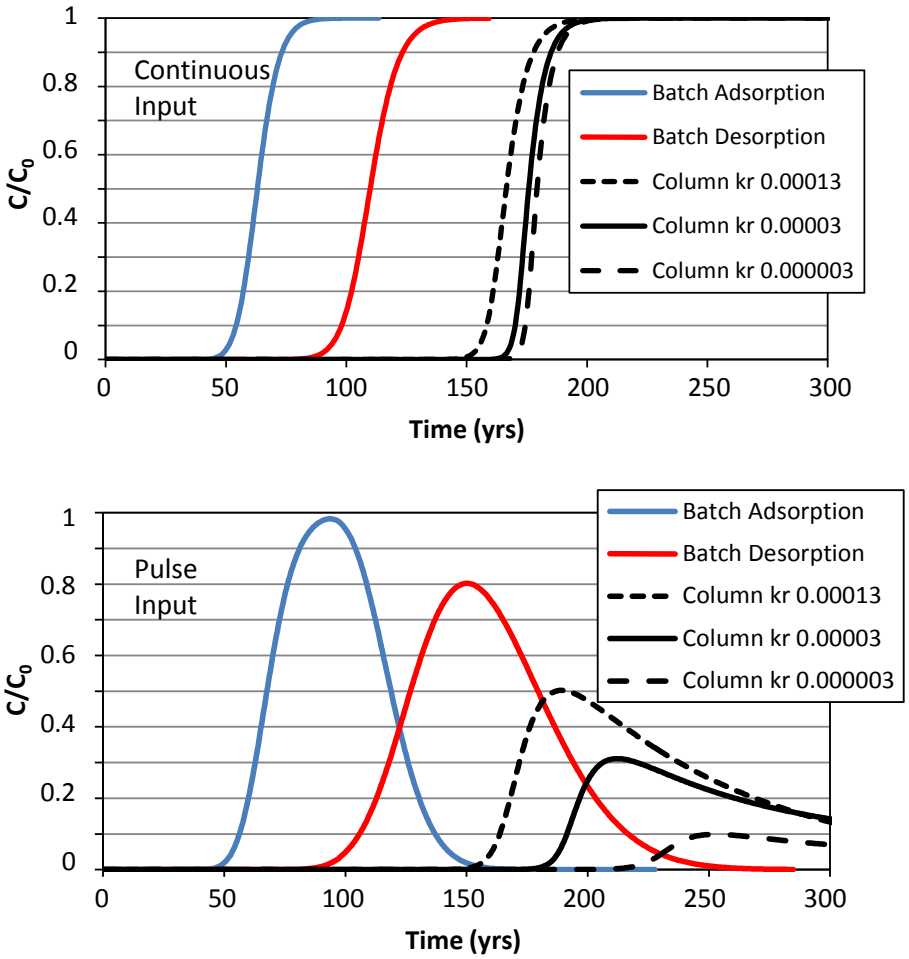

Figure 6. Uranium transport predictions over large scales at pH 6.9 using one-site model with partition coefficients from batch experiments (blue and red) and three-site model with reaction rate constants from column experiments (black). Mean water residence time is one year and U input concentration is 6.5 μM. Top plot shows response to continuous U input and bottom plot show response to a 50-year pulse input. k_r values in legend are desorption rate constant of third sorption site.

The curves generated using the column parameters have significantly greater U retardation factors than either of the curves generated using the batch K_d values. Also, while the response to a continuous U input is relatively insensitive to the desorption rate constant of the third site, the response to a 50-year-pulse input shows considerable sensitivity to this parameter. We attribute the latter behavior to a greater influence of the low-abundance third site when the average U concentration is lower, as it is when the input function is of limited duration. The continuous injection of U tends to saturate the less-abundant third site and thus lessens the influence of the desorption rate constant.

Figure A6 shows the results of the large-scale model simulations at pH 7.9. The same assumptions were used as in the pH 6.9 simulations except the finite pulses in the lower plot were 10 years instead of 50 years. The column parameters predict a U retardation factor that is greater than the one-site simulation using the batch adsorption K_d value but less than the simulation using the batch desorption K_d value.

The reason for the different behavior at pH 7.9 compared to pH 6.9 is attributed to the similarity of the ratios of the adsorption to desorption rate constants for all three sites at pH 7.9 and also to the smaller range of the desorption rate constants and the greater value of the slowest desorption rate constant at this pH. In effect, all three sites have similar individual partition coefficients at pH 7.9, with the only difference being their relative adsorption and desorption rates. These characteristics all contribute to well-behaved transport that is consistent with a single partition coefficient at large scales (i.e., when the time scale is large compared to the time scales of all the reactions). In contrast, at pH 6.9 the third site has a significantly greater ratio of adsorption to desorption rate constant and hence a greater effective partition coefficient than the other two sites. This disparity, coupled with the limited number of slower sites and the very

small desorption rate constant of the third site gives rise to greater retardation relative to that predicted from the batch experiments and also to a large sensitivity of the pulse input breakthrough curves to the third-site desorption rate constant.

At pH 6.9, the desorption rate constant of the third site has the largest effect on the large-scale transport behavior of U. This is also the most uncertain and most difficult parameter to estimate. The adsorption site densities are also somewhat uncertain, but their impact is lessened by the negative correlation between the adsorption rate constant and the site density. This negative correlation tends to be self-compensating because sites that have smaller densities tend to have larger adsorption rate constants to match the same experimentally-observed rates and amounts of adsorption. Nonetheless, obtaining better constraints on site densities would reduce uncertainties in larger-scale transport predictions. It is worth noting that the column experiments imposed some loose lower limit constraints on surface densities of the slower sites because the fits degraded as surface densities were decreased below certain values (a point was reached where increasing the adsorption rate constants of these sites could no longer compensate for the decreased surface densities).

A very small number of sites that are effectively irreversible (zero desorption rate constant) could have a dramatic influence on large-scale transport predictions provided that plume concentrations and pulse durations remain low enough that irreversible sites do not become saturated. Although it is technically not possible to measure desorption rates of zero (we can only place upper limits on very low rates), the lack of complete recovery predicted by conservative log-log extrapolations of the tails of the U breakthrough curves in the pH 6.9 column experiments suggests that there may be some desorption rates that are low enough at this pH to have a very significant impact on the large-scale transport of U. Interrogating these slow

desorption rates, while difficult, has a large effect on improving (and removing conservatism from) large-scale transport predictions. Overall, the relatively small surface area of the FFM and limited number of binding sites shows that the FFM is not as effective as engineered barrier materials at attenuating U transport.

5. Conclusions

Through the experiments and interpretive models described in this paper, we demonstrate a method of interrogating slow desorption rates to improve reactive transport predictions over long time and distance scales. Batch experiments proved useful in predicting early U breakthrough in the column while breakthrough columns allowed for interrogation of the relationship and relative importance of different sorption sites in transport. This approach could be applied to any moderately-sorbing radionuclide in any hydrogeologic system to reduce conservatism in large-scale predictions. The most important improvement would be to carry out the flushing phase of the column experiments (at the same solution conditions as the injection/loading phase) until curvature is observed in the log-linear tailing of the breakthrough curves or until detection limits are reached. This would allow the lowest possible estimates of the *upper limits* of slow desorption rate constants, which are important for safe and economical repository designs. Introducing flow interruptions during the log-linear tailing portions of the breakthrough curves would also provide better constraints on very slow desorption rates.

A three-site kinetic model yielded good fits to the U column transport data at pH 6.9 and 7.9 and could easily be implemented in performance assessment models with little additional computational burden over a simple linear partition coefficient (K_d) model. This approach is consistent with multirate models, although we believe that three sites are probably sufficient to explain most experimental data sets and that it is not necessary (and less defensible) to employ

continuous distributions of rate constants. We also believe it is not necessary or defensible to constrain all the sites to have the same effective partition coefficient. A three-site kinetic model is also consistent with more sophisticated geochemical modeling approaches where U transport has been shown to be effectively simulated using three types of surface complexation sites (weak, strong and very strong) in a classic geochemical modeling framework. When the ratio of the adsorption to desorption rate constants of all sites are similar in magnitude and the time scale of the slowest desorption reaction is fast relative to the time scale of transport, a simple linear partition coefficient (K_d) approach can be effectively used to describe reactive transport over long time and distance scales.

Supplementary Materials

Appendix A contains additional tables and figures for water chemistry, experimental data, and model fits including SGGW solution recipe (Table A1), PHREEQC uranium speciation (Table A2), model reaction parameters (Table A3), retardation coefficients (Table A4), image of set-up (Fig. A1), plots of control column data (Fig. A2), pH 6.9 column data (Fig. A3), pH 7.9 column data (Fig. A4), batch experimental data fit with column parameters (Fig. A5), and pH 7.9 large scale model prediction plots (Fig. A6).

Acknowledgements

The authors would like to thank Doug Ware for his assistance with experimental setup, liquid scintillation counting protocols, sample analysis, and microphotograph imagery. We also thank Cindy Dean for the PHREEQC calculations of U speciation in the SGGW at the different pHs, and Ingo Blechschmidt of the Swiss Nuclear Waste Cooperative, NAGRA, for providing the granodiorite and FFM materials. This work was supported by the U.S. DOE Nuclear Energy

Office, Fuel Cycle R&D Program, Used Fuel Disposition Campaign, which is administered by Sandia National Laboratories.

References

Boukhalfa, H., Dittrich, T., Reimus, P., Ware, D., Erdmann, B., Wasserman, N., Abdel-Fattah, A. 2013. Plutonium and cesium colloid mediated transport. Abs., EOS, Trans. Amer. Geophys. Union, 94: H21E-1111. Presented at the American Geophysical Union Fall Meeting, San Francisco, CA, December 9.

Davis, J.A., Curtis, G.P., 2003. Application of Surface Complexation Modeling to Describe Uranium(VI) Adsorption and Retardation at the Uranium Mill Tailings Site at Naturita, Colorado, NUREG/CR-6820, United States Geological Survey (for Nuclear Regulatory Commission), Menlo Park, CA.

Davis, J.A., Meece, D.E., Kohler, M. Curtis, G.P., 2004. Approaches to surface complexation modeling of uranium(VI) adsorption on aquifer sediments. Geochim. Cosmochim. Acta 68, 3621-3641.

Davis, J.A., Ochs, M., Olin, M., Payne, T.E., Tweed, C.J., 2005. NEA Sorption Project Phase II-Interpretation and Prediction of Radionuclide Sorption onto Substrates Relevant for Radioactive Waste Disposal Using Thermodynamic Sorption Models. Nuclear Energy Agency, Paris.

Dittrich, T.M., Boukhalfa, H., Ware, S.D., Reimus, P.W., 2015a. Laboratory investigation of the role of desorption kinetics on americium transport associated with bentonite colloids. J. Environ. Radioactiv. 148, 170-182. doi: 10.1016/j.jenvrad.2015.07.001

Dittrich, T.M., Boukhalfa H., Reimus, P.W., 2015b. Three column series approach to investigate role of desorption rates in colloid-facilitated transport of americium, cesium, and plutonium: Experiments and modeling. Abstr. Pap. Am. Chem. Soc. 249, 249th American Chemical Society National Meeting, Denver, CO, Mar 25, American Chemical Society: Washington, D.C, 2015; 455-COLL. LA-UR-15-22155.

Dittrich, T.M., Reimus, P.W., 2015. Uranium transport in a crushed granodiorite: Experiments and reactive transport modeling. J. Contam. Hydrol. 175-176, 44-59. doi: 10.1016/j.jconhyd.2015.02.004.

Dittrich, T.M., Ware, S.D., Reimus, P.W., 2015c. Mini-columns for conducting breakthrough experiments: Design and construction. LA-UR-15-24392; Los Alamos National Laboratory, Los Alamos, NM. doi: 10.2172/1184604

Dittrich, T.M., Reimus, P.W., 2014. Potential for colloid-facilitated transport of americium in a bentonite/granodiorite system. Abstr. Pap. Am. Chem. Soc. 247, 247th American Chemical Society National Meeting, Dallas, TX, Mar 18, American Chemical Society: Washington, D.C, 2014; 113-GEOC. LA-UR-14-21928.

Dittrich, T.M., Reimus, P.W., 2013. Experimental evaluation of actinide transport in a fractured granodiorite. Proceedings of the 14th International High-Level Radioactive Waste Management Conference, American Nuclear Society, LaGrange Park, IL. pp. 473-480.

Doherty, J.E., 2009. Manual for PEST: Model Independent Parameter Estimation, in: J.E. Doherty (Ed.). Watermark Numerical Computing, Brisbane, Australia, p. 336.

Doherty, J.E., 2010. Addendum to the PEST Manual, in: J.E. Doherty (Ed.). Watermark Numerical Computing, Brisbane, Australia, p. 131.

Dong, W., Brooks, S., 2006. Determination of the formation constants of ternary complexes of uranyl and carbonate with alkaline earth metals (Mg^{2+}, Ca^{2+}, Sr^{2+}, and Ba^{2+}) using anion exchange method. Environ. Sci. Technol. 40, 4689–4695.

Dong, W., Wan, J., 2014. Additive surface complexation modeling of uranium(VI) adsorption onto quartz-sand dominated sediments. Environ. Sci. Technol. 48, 6569-6577.

Echevarria, G., Sheppard, M. I., Morel, J. L., 2001. Effect of pH on the sorption of uranium in soils. J. Environ. Radioactiv. 53, 257-264.

ENRESA, 1998. FEBEX, Full-scale Engineered Barriers Experiment in crystalline host rock – Pre-operational stage summary report, Technical Publication 01/98, Madrid, Spain.

Giammar, D. E., Hering, J. G., 2001. Time scale for sorption-desorption and surface precipitation of uranyl on Goethite. Environ. Sci. Technol. 35, 3332–3337.

Good, N. E., Winget, G. D., Winter, W., Connolly, T. N., Izawa, S., Singh, R. M. M. 1966. Hydrogen ion buffers for biological research. Biochemistry 5, 467-477.

Huber, F., Kunze, P., Geckeis, H., Schäfer, T., 2011. Sorption reversibility kinetics in a ternary system radionuclide – bentonite colloids/nanoparticles – granite fracture filling material. Appl. Geochem. 26**,** 2226-2237.

Johnson, J., 2010. llnl.dat 4023 2010-02-09. Data from 'thermo.com.V8.R6.230' prepared by Jim Johnson at Lawrence Livermore National Laboratory, in Geochemist's Workbench format. Converted to PHREEQC format by Greg Anderson with help from David Parkhurst.

Joseph, C., Stockmann, M., Schmeide, K., Sachs, S., Brendlet, V., Bernhard, G., 2013. Sorption of U(VI) onto Opalinus clay: Effects of pH and humic acid. Appl. Geochem. 36, 104-117.

Kersting, A., Zavarin, M., Zhao, P., Dai, Z. Carroll, S., Wang, Y., Miller, A., James, S., Reimus, P., Zheng, L., Li, L., Rutqvist, J., Liu, H.-H., Birkholzer, J., 2012. Radionuclide Interaction and Transport in Representative Geologic Media, Used Fuel Disposition Campaign Milestone Report FCRD-UFD-2012-000154; Chapter 5, Laboratory Testing Complementing Grimsel Field Work: Conservative Tracer Screening and Preliminary Radionuclide Transport Experiments.

Liu, C., Zachara, J. M., Qafoku, N. P., Wang, Z., 2008. Scale-dependent desorption of uranium from contaminated subsurface sediments. Water Resour. Res. 44(8), doi: 10.1029/2007WR006478.

Missana, T., Garcia-Gutierrez, M., Alonso, U., 2004. Kinetics and irreversibility of cesium and uranium sorption onto bentonite colloids in a deep granitic environment. Appl. Clay Sci. 26, 137-150.

Mohanty, S.K., Saiers, J.E., Ryan, J.N., 2014. Colloid-facilitated mobilization of metals by freeze thaw cycles. Environ. Sci. Technol. 48, 977-984.

Morel F.M.M., Hering, J.G., 1993. Principles and Applications of Aquatic Chemistry. Wiley-Interscience, New York.

Nebelung, C., Brendler, V., 2010. U(VI) sorption on granite: predictions and experiments. Radiochim. Acta 98, 621-625.

Parkhurst, D.L., Appelo, C.A.J., 2013. PHREEQC (Version 3.0.4) - A computer program for speciation, batch speciation, one-dimensional transport, and inverse geochemical calculations, U.S. Geological Survey Techniques and Methods, Book 6, Chapter A43, p. 497, http://pubs.usgs.gov/tm/06/a43/.

Payne, T.E., Brendler, V., Ochs, M., Baeyens, B., Brown, P.L., Davis, J.A., Ekberg, C., Kulik, D.A., Lutzenkirchen, J., Missana, T., Tachi, Y., Van Loon, L.R., Altmann, S., 2013. Environ. Modell. Softw. 42, 143-156.

Tsang, Y. W., 1995. Study of alternative tracer tests in characterizing transport in fractured rocks, Geophys. Res. Letters 22, 1421-1424.

Waite, T.D., Davis, J.A., Fenton, B.R., Payne, T.E., 2000. Approaches to modelling uranium(VI) adsorption on natural mineral assemblages. Radiochim. Acta 88, 687-693.

Waite, T. D., Davis, J. A., Payne, T. E., Waychunas, G. A., Xu, N., 1994. Uranium(VI) adsorption to ferrihydrite – Application of a surface complexation model. Geochim Cosmochim. Acta 58, 5465-5478.

Wang, Y., Matteo E., Rutqvist, J., Davis, J., Zheng, L.,Houseworth, J., Birkholzer, J., Dittrich, T., Gable, C., Karra, S., Makedonska, N., Chu, S., Harp, D., Painter, S., Reimus, P., Perry, F., Zhao, P., Begg, J., Zavarin, M., Tumey, S., Dai, Z., Kersting, A., Jerden, J., Frey, K., Copple, J.M., Ebert, W. 2014a. Used Fuel Disposal in Crystalline Rocks: Status and FY14 Progress, Used Fuel Disposition Campaign Milestone Report FCRD-UFD-2014-000060 and SAND2014-17992R; Chapter 5, Describing Uranium Transport in a Fractured Crystalline Rock Using Mini-Column Experiments. pp. 147-180.

Wang, Y., Matteo E., Rutqvist, J., Davis, J., Zheng, L.,Houseworth, J., Birkholzer, J., Dittrich, T., Gable, C., Karra, S., Makedonska, N., Chu, S., Harp, D., Painter, S., Reimus, P., Perry, F., Zhao, P., Begg, J., Zavarin, M., Tumey, S., Dai, Z., Kersting, A., Jerden, J., Frey, K., Copple, J.M., Ebert, W. 2014b. Used Fuel Disposal in Crystalline Rocks: Status and FY14 Progress, Used Fuel Disposition Campaign Milestone Report FCRD-UFD-2014-000060 and SAND2014-17992R; Chapter 6, Laboratory Investigation of Colloid-Facilitated Transport of Americium by Bentonite Colloids in a Granodiorite System. pp. 181-200.

Wang, Y. Gardner., P., Reimus, P., Painter, S., Makedonska, N., Pollack, A., Houseworth, J., Rutqvist, J., Asahina, D., Chen, F., Vilarrasa, V., Liu, H., Birkholzer, J., Begg, J., Zavarin, M., Kersting, A., Kim, G., 2013a. Natural System Evaluation and Tool Development – International Collaborations: FY13 Progress Report, Used Fuel Disposition Campaign Milestone Report FCRD-UFD-2013-000628; Chapter 2, Interpretations of Colloid-Facilitated Transport Experiments at the Grimsel Test Site from 2008 through 2012. pp. 5-42.

Wang, Y., Miller, A., Matteo, E., Reimus, P., Ding, M., Dittrich, T., Zheng, L., Houseworth, J., Zhao, P., Kersting, A., Dai, Z., Zavarin, M., 2013b. Experimental and Modeling Investigation of Radionuclide Interaction and Transport in Representative Geologic Media, Used Fuel Disposition Campaign Milestone Report FCRD-UFD-2013-000314; Chapter 5,

An Experimental Methodology for Improving Radionuclide Transport Process Models using Uranium and Grimsel Granodiorite as a Case Study. pp. 47-76.

Tables

Table 1. Summary of column experimental conditions.

Injection Solution (pH 6.9)	Approximate Start Time (h)	Approximate Start Volume (ml)
6.5 μM U, pH 6.9	0	0
U-free SGGW, pH 6.9	834	228
U-free SGGW, pH 9.0	3412	736
0.1 M HCl, pH 1.2	5202	1226
Injection Solution (pH 7.9)		
6.5 μM U, pH 7.9	0	0
U-free SGGW, pH 7.9	467	128
0.1 M HCl, pH 1.2	2456	476

a Volumes and times varied slightly between duplicate columns

b Flow rate in all columns was approximately 0.28 mL h^{-1}

Table 2. Reactive transport parameter estimates providing the best three-site model fit to the uranium breakthrough curves at pH 6.9 (Fig. 1).

Starting Vol. (ml)	Adsorption Site	k_f (ml/g-h)	k_r (h^{-1})	S_m (μmol/g)
0	**1**	2.1	0.07 (0.06)[a]	1.3[b]
(pH 6.9)	**2**	0.07	0.0022	0.39
	3a	0.007	0.00003	0.104
	3b	0.001	0.00003	0.026
736	**1**	0.1	0.06	1.3[b]
(pH 9 flush)	**2**	0.02	0.0035	0.39
	3a	0.0018	0.00011	0.104
	3b	0.0002	0.00011	0.026
1226	**1**	0.01	0.1	1.3[b]
(pH 1 flush)	**2**	0.003	0.2	0.39
	3a	0.0001	0.2	0.104
	3b	0.0001	0.013	0.026

[a] Value in parentheses was used after uranium-free water was introduced at ~228 ml.

[b] Model is insensitive to surface density of first site as long as it is greater than 1.3 μmol/g.

Table 3. Reactive transport parameter estimates providing the best three-site model fit to the uranium breakthrough curves at pH 7.9 (Fig. 2).

Adsorption Site	k_f (ml/g-h)	k_r (h^{-1})	S_m (μmol/g)
1	0.5	0.12	1.3[a]
2	0.014	0.0058	0.39
3	0.0035	0.0007	0.104

[a] Model is insensitive to surface density of first site as long as it is greater than 1.3 μmol/g.

Table 4. Experimentally-observed partition coefficients (K_d values) in batch experiments based on final concentrations measured during adsorption and desorption phases of experiments.

pH 6.9	Adsorption K_d (ml/g)	Desorption K_d (ml/g)
1g : 10 ml	24.0	46.2
0.5 g : 10 ml	26.7	46.0
0.2 g : 10 ml	24.0	60.3
pH 7.9	**Adsorption K_d (ml/g)**	**Desorption K_d (ml/g)**
1g : 10 ml	5.3	14.4
0.5 g : 10 ml	8.6	20.9
0.2 g : 10 ml	11.3	60.1

Supplementary Materials

Appendix A. Water Chemistry and Experimental Data Tables and Figures

Table A1. Synthetic Grimsel groundwater (SGGW) recipe.

Compound	mg L^{-1}
Na_2SO_4	144
KCl	5
$MgCO_3$	43
$NaHCO_3$	27
$CaCl_2$	13
H_4SiO_4	34

Table A2. Percent abundance of uranium-bearing species in SGGW as a function of pH (from PHREEQC).

Constituent	pH 6.9	pH 7.9
$UO_2Ca(CO_3)_3^{2-}$	47.8	56.2
$UO_2Mg(CO_3)_3^{2-}$	18.1	21.7
$UO_2(CO_3)_2^{2-}$	14.1	1.7
$UO_2Ca(CO_3)_2$	8.7	10.0
$UO_2(CO_3)_2^{4-}$	7.9	9.4
$UO_2(CO_3)$	1.8	<0.1
$UO_2Mg_2(CO_3)_3$	0.8	<0.1
$UO_2(OH)^+$	<0.1	<0.1
UO_2^{2+}	<0.1	<0.1
Mass Balance	99.2	99.0

Table A3. Reaction model parameters yielding matches to FFM batch adsorption-desorption data shown in Fig. 3.

pH 6.9	k_f **(ml/g-h)**	k_r **(h^{-1})**	S_m **(μmol/g)**
1-site model	0.3	0.005	1.3[a]
3-site model, site 1	0.8	0.06	1.3[a]
3-site model, site 2	0.1	0.003	0.104
3-site model, site 3	0.07	0.001	0.026
pH 7.9			
3-site model, site 1	0.8	0.4	1.3[a]
3-site model, site 2	0.05	0.005	0.039
3-site model, site 3	0.05	0.001	0.013

[a] Model is insensitive to surface density of first site as long as it is greater than 1.3 μmol/g.

Table A4. Comparison of retardation coefficients predicted from batch adsorption partition coefficients (Table 4) with retardation coefficients observed in column experiments (leading edge of breakthrough curves).

pH 6.9	Batch Ret. Coef.	Column Ret. Coef.
1g : 10 ml	64.6	
0.5 g : 10 ml	71.1	80
0.2 g : 10 ml	64.6	
pH 7.9	**Batch Ret. Coef.**	**Column Ret. Coef.**
1g : 10 ml	15.1	
0.5 g : 10 ml	23.8	10.3
0.2 g : 10 ml	30.9	

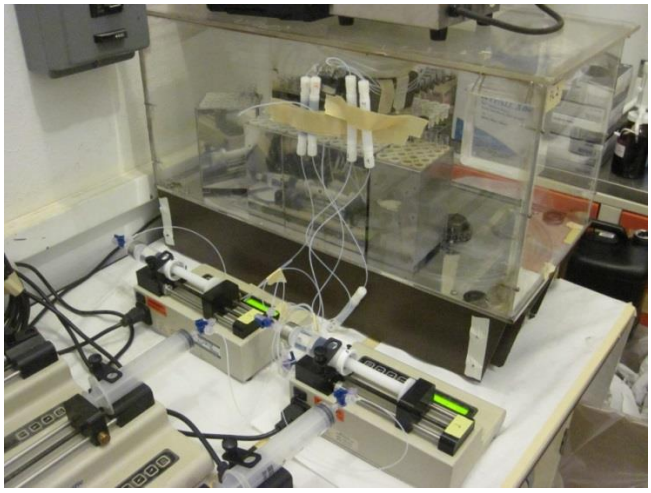

Figure A1. Image of column set-up with 4 columns running in parallel with syringe pumps, tubing, and fraction collector.

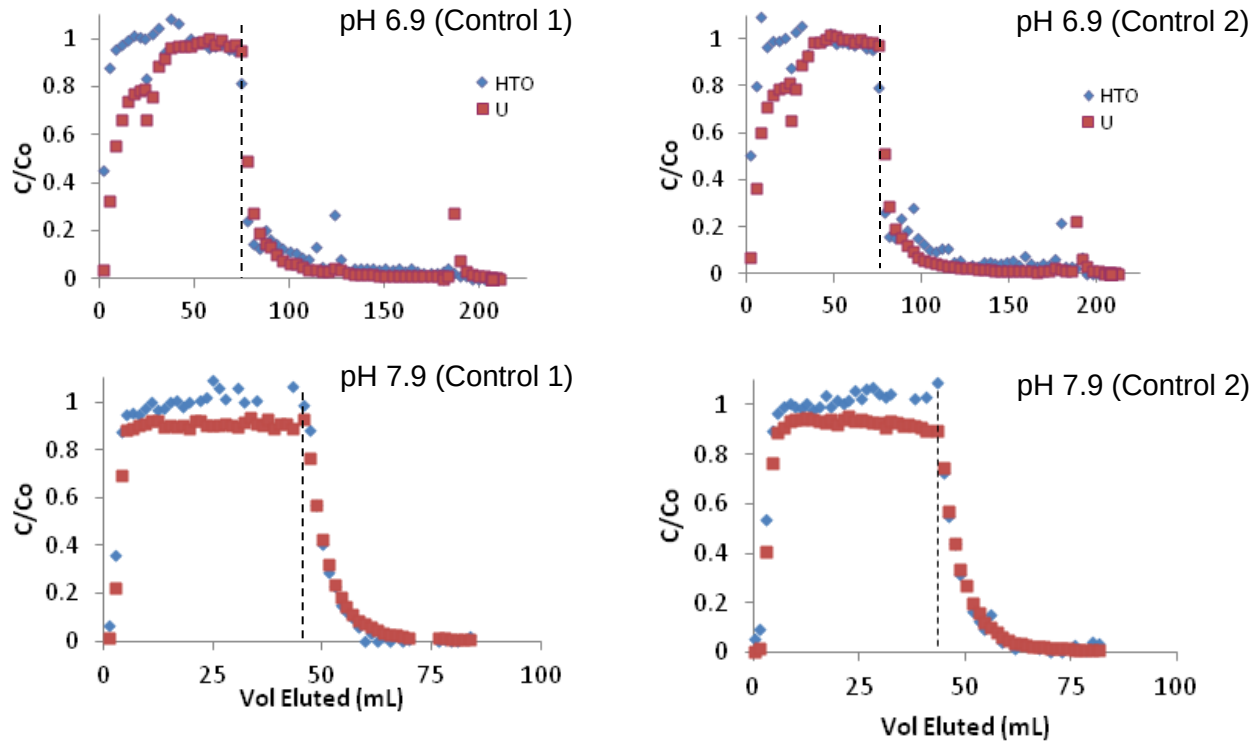

Figure A2. Control breakthrough experiments without FFM for duplicate columns with uranium solutions of pH 6.9 (top) and pH 7.9 (bottom). Dashed lines denote when injection solution was switched to uranium- and tritium-free solution.

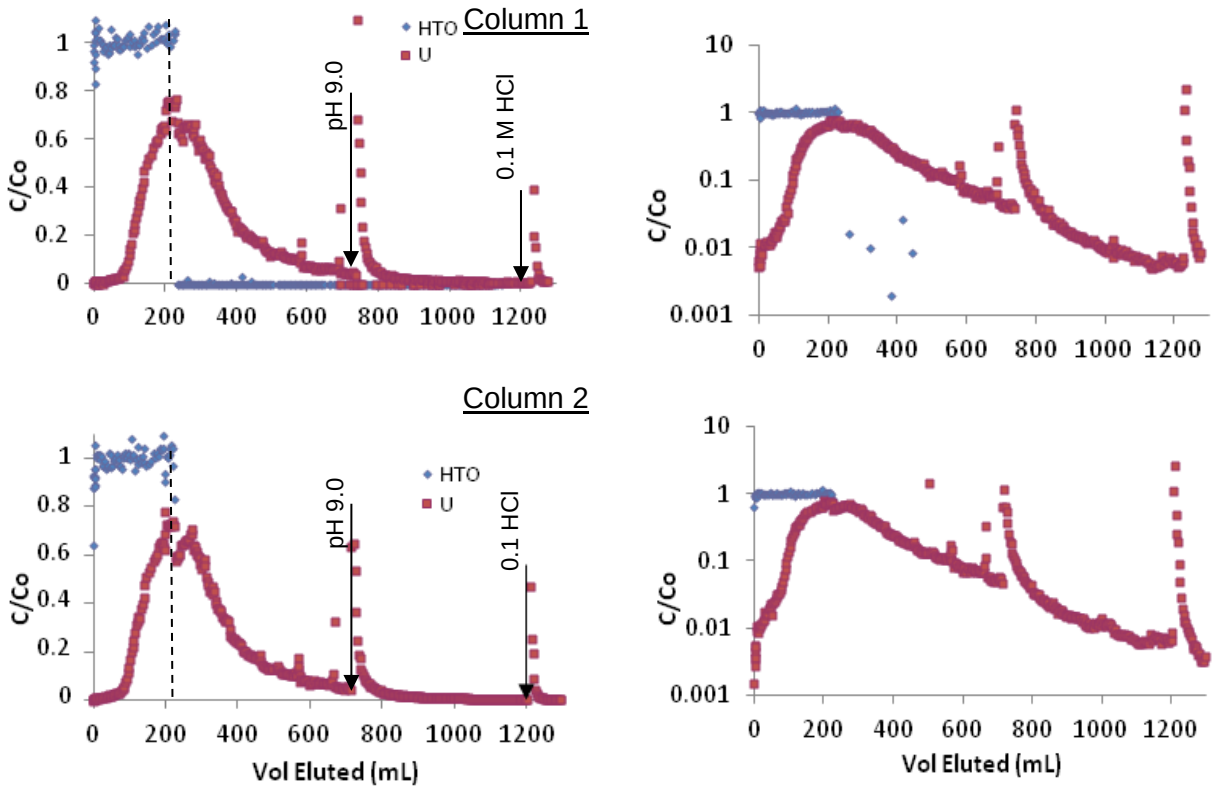

Figure A3. Breakthrough curves for duplicate FFM breakthrough experiments with pH 6.9 uranium solutions pl linear concentration scale (left) and logarithmic scale (right) to highlight the desorption behavior. Dashed lines d injection solution was switched to uranium- and tritium-free solution.

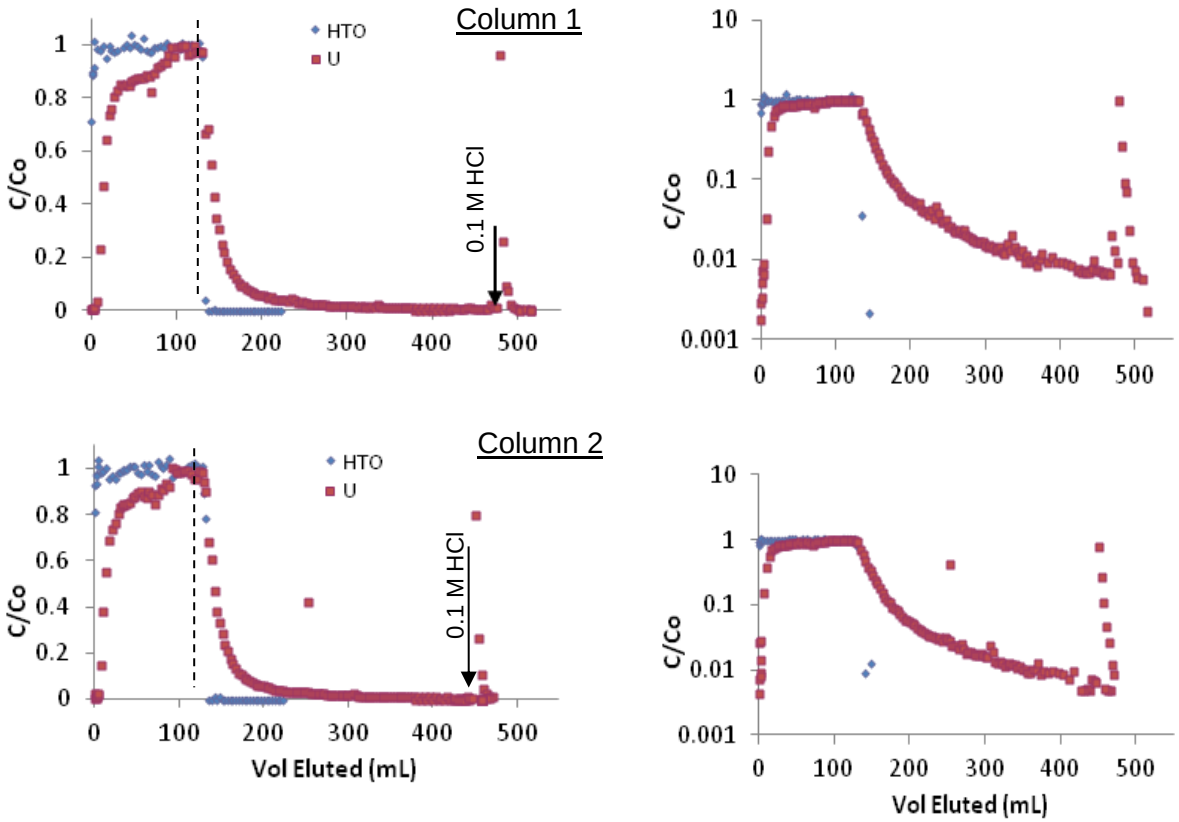

Figure A4. Breakthrough curves for duplicate FFM breakthrough experiments with pH 7.9 uranium solutions pl linear concentration scale (left) and logarithmic scale (right) to highlight the desorption behavior. Dashed lines c injection solution was switched to uranium- and tritium-free solution.

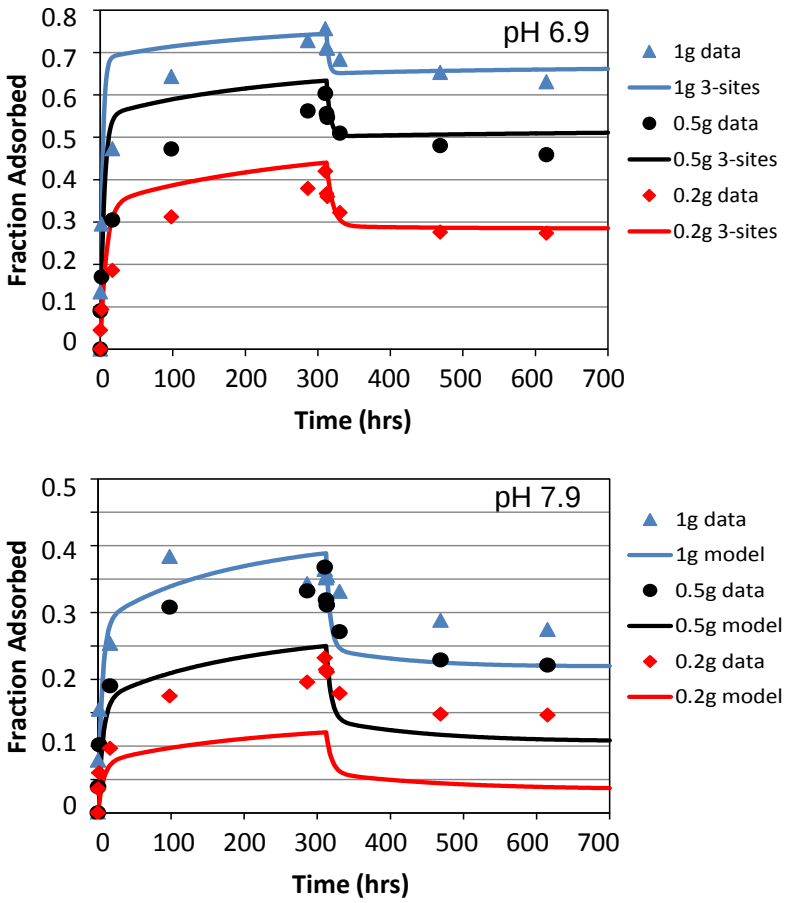

Figure A5. FFM batch adsorption and desorption data at pH 6.9 (top) and pH 7.9 (bottom), showing 3-site model predictions using the best-fitting reaction parameters from the column experiments.

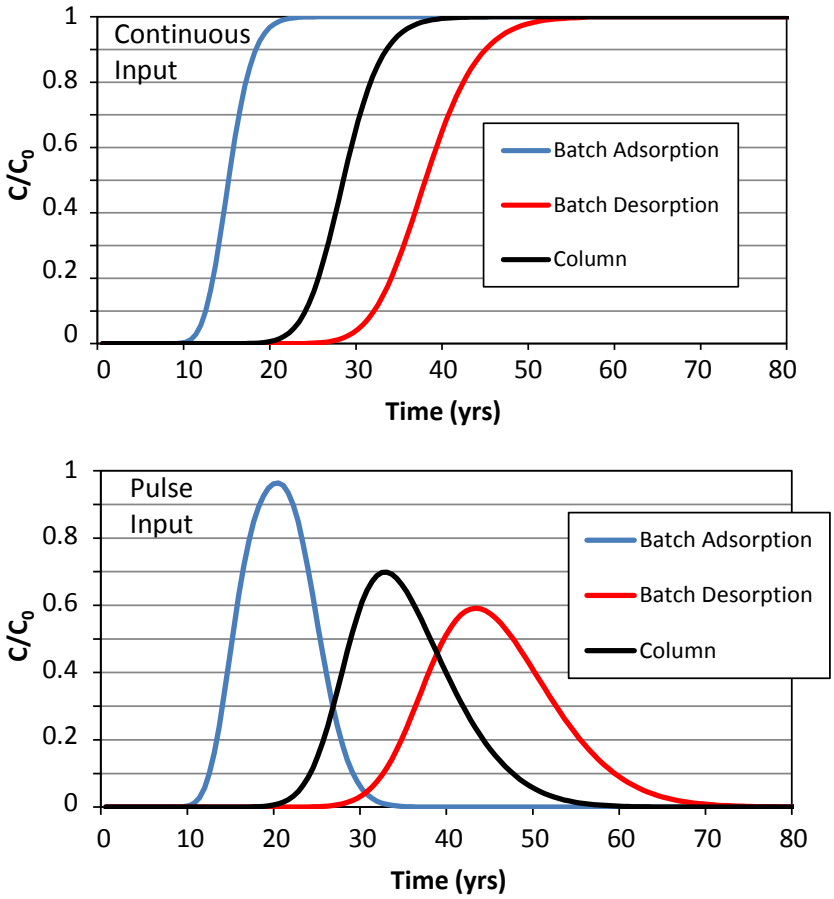

Figure A6. Uranium transport predictions over large scales at pH 7.9 using one-site model with partition coefficients from batch experiments (blue and red) and three-site model with reaction rate constants from column experiments (black). Mean water residence time is one year and uranium input concentration is 6.5 μM. Top plot shows response to continuous uranium input and bottom plot show response to a 50-year pulse input.